CrossMark

RESEARCH PAPER

A study of the micro-mechanical properties of butt fusion-welded joints in HDPE pipes using the nanoindentation technique

Muhammad Shaheer[1] · Mike Troughton[2] · Amir Khamsehnezhad[2] · Jim Song[1]

Abstract High-density polyethylene (HDPE) pipes are being used increasingly in many traditional industries as an alternative to metallic pipes. The weakest part of every pipe system is the welded joint. A number of standards are available that define the welding procedure for butt fusion welding of HDPE pipes. However, they define very different values for welding pressure and temperature, for the exact same materials. HDPE PE100 180 mm SDR11 pipes were welded using various standard and non-standard welding procedures. The ranges of welding parameters chosen were expected to produce detectable changes in the size of the weld regions and their micro-mechanical properties. The micro-mechanical properties across butt fusion welds were characterised using the nanoindentation technique. The indentations were spaced at 100 μm at the mid-wall position of the welded joint in a grid of 60 columns by 3 rows. The melt zone (MZ) showed a distinct drop in material properties consistently across all welding procedures. Nanoindentation also revealed the presence of a heat-affected zone (HAZ) surrounding the MZ, characterised by a gradual increase in material properties from that of the parent material to the boundary with the MZ. The size of the MZ measured using nanoindentation was correlated with transmission light microscopy images of microtomed slices.

Abbreviations

DSC	Differential scanning calorimetry
DVS	German Welding Society
FEA	Finite element analysis
HAZ	Heat-affected zone
HDPE	High-density polyethylene
ISO	International Standards Organisation
MZ	Melt zone
NI	Nanoindentation
PPI	Plastic Pipe Institute
SDR	Standard dimension ratio
TLM	Transmission light microscopy
WIS	Water Industry Specification.

✉ Muhammad Shaheer
  Muhammad.shaheer@brunel.ac.uk

1 Brunel University London, Kingston Lane, Uxbridge, Middlesex UB8 3PH, UK

2 TWI Ltd., Granta Park, Great Abington, Cambridge CB21 6AL, UK

1 Introduction

One of the leading pipeline materials for the transport of gas and water has been high-density polyethylene (HDPE). HDPE pipes have been replacing traditionally used lead and iron pipes due to their properties such as high chemical and corrosion resistance, and low weight, which lowers the costs of production, transportation, and installation [1]. Since HDPE is a thermoplastic, almost all methods of joining rely on heat to induce a thermally agitated phase change and pressure to

molecularly mix the parent materials to form a weld. Despite the advances in material processing and welding technology, not all of the weld material properties match the parent material properties [2]. A micro-structural-level understanding is lacking regarding the weld geometry and properties and how the weld interacts with the parent material. Nanoindentation is one of the few techniques that enable the investigation of the micro-mechanical properties of HDPE pipe welds. For this reason, this technique was used to characterise the micro-structure of these welds in order to improve the fundamental understanding of how polymer welding processes affect the weld micro-structure, which would be highly beneficial in advancing the reliability and performance of HDPE piping systems.

1.1 Welding

Butt fusion welding is a common joining method for welding of HDPE pipes. A typical butt fusion-welding procedure involves the following steps: the pipe ends are aligned and trimmed flat before being pressed against a heater plate, which is at a temperature of 70–100 °C above the melting point of HDPE, until the onset of melting is visible by the formation of melt beads, the pipes are separated and the heater plate is removed; the melted pipe ends are then brought together under pressure and allowed to cool at ambient temperature. A weld is formed as the material in the melt zone (MZ) undergoes molecular interpenetration and recrystallises under external axial stress. There are several standards around the world that define butt fusion-welding procedures using a range of values for welding parameters such as pressure, temperature, and time.

1.2 Nanoindentation

Nanoindentation (NI) is a translation of macroscale hardness testing through indentation to nanoscale [3, 4]. Several of the earliest hardness mechanical techniques, precursor to NI, are now over 100 years old. However, technological

developments in the early 1970s have enabled extraction of material properties such as the elastic modulus in the sub-micron range. The NI technique involves using a very hard (usually synthetic diamond based) indenter of a known geometry to perform indentations whilst very accurately measuring force and depth [5]. The load-displacement curve is used, in conjunction with the material properties and geometry of the indenter, to derive the material properties of the material under test [6].

2 Methodology

2.1 Material

The black HDPE pipe used in this study had an outer diameter of 180 mm and minimum wall thickness of 16.4 mm (SDR11) and was made from BorSafe™ HE-3490-LS PE100 resin. Some of the physical properties from the manufacturer's material data sheet are listed in Table 1.

2.2 Welding

Six different welding procedures, listed in Table 2, were used to produce 1-m-long welded pipes with the weld at 0.5 m position. Four of the six procedures are defined in standards used worldwide [8]. The remaining two procedures were used to investigate the effect of extreme welding temperatures at high welding pressures. It was expected that the weld micro-structure and micro-mechanical properties would differ due to the different sets of welding parameters.

A dummy weld was produced before the welding took place for each procedure to ensure that no contamination from the hot plate was transferred to the weld, in order to produce consistent weld quality. The welding for the Water Industry Specification (WIS) and German Welding Society (DVS) procedures (WP1-2) was carried out using a Fusion Provida BF315 butt fusion-welding machine, and the remaining procedures (WP3-6) were carried out using a McElroy MC250EP machine. It

Table 1 HE-3490-LS product data sheet [7]

Physical properties		Typical value	Unit	Test method
Density	Base resin	949	kg/m^3	ISO 1183/ISO 1872-2B
	Compound	959		
Tensile stress at yield	50 mm/min	25	MPa	ISO 527–2
Tensile strain at break		>600	%	ISO 527–2
Tensile modulus	1 mm/min	1100	MPa	ISO 527–2
Charpy impact, notched	0 °C	16	kJ/m^2	ISO 179/1eA
Hardness, shore D		60		ISO 868
Resistance to slow crack growth	9.2 bar, 80 °C	>1000	h	ISO 13479
Thermal stability	210 °C	>20	min	EN 728

Table 2 Welding parameters of the six welding procedures

Welding procedure		Interfacial pressure (MPa)	Heater plate temperature (°C)	Heat soak time (s)	Fusion/cooling time (s)
WP1	WIS 4–32-08	0.15	230	225	600
WP2	DVS 2207–1	0.15	218	165	1200
WP3	PPI TR-33 ideal	0.517	218	435	450
WP4	PPI TR-33 acceptable	0.621	232	382	450
WP5	High pressure, low temperature	0.827	177	821	450
WP6	High pressure, high temperature	1.034	260	257	450

was not possible to use the same machine to produce welds for all welding procedures as only the former machine was certified for WIS and DVS procedures, and only the latter machine could achieve the specified higher welding pressures.

2.3 Nanoindentation

The very high spatial resolution of the NI technique has been used to measure the variability of the material properties across the HDPE welds. The NI specimens, with the weld in the centre, were cut from the butt fusion joint with the weld bead intact (Fig. 1a). These specimens, measuring 25 mm in length by 25 mm in width, were machined to ensure that the indentation surface was parallel to the back of the specimen (Fig. 1b). The test surfaces of each specimen were then ground and polished with successively finer grades of abrasive silicon carbide paper to achieve an average surface roughness of 2.5 μm [9, 10]. An indentation grid was placed at the centre of the pipe wall across the weld region as shown in Fig. 2 for each specimen. The grid consisted of 60 columns by 3 rows of indents, spaced 100 μm apart. The nanoindentation parameters are listed in Table 3.
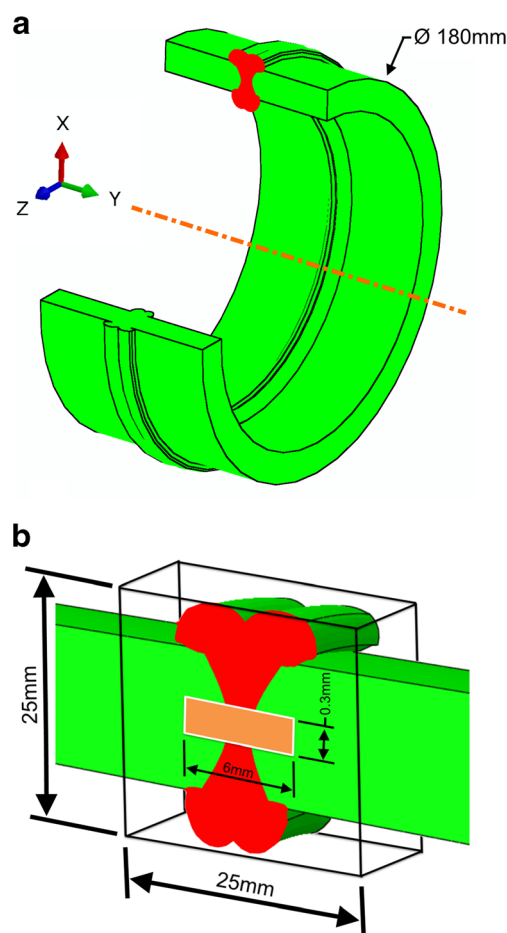
2.4 Finite element analysis

Finite element analysis (FEA) was used to model the heat transfer and the temperature profile during the heating cycle. Only half the 1-m-long pipe was modelled as it was considered symmetrical about the weld interface. Thermal modelling of the heating cycle of the welding process was carried out using an axisymmetric pipe geometry in Abaqus 6.13–1. The modelling only accounted for conductive heat transfer as it has the largest contribution. The interfacial pressure was not modelled in order to reduce the complexity of the thermal model. Therefore, no bead was formed and the pipe did not experience any deformation. The cooling cycle lasted for 600 s after which the model terminated. The temperature distribution was recorded using a path of 25 points spaced 1 mm apart from the heated pipe end, at the centre of the pipe wall. The mesh density was 1 mm^2 using 8000 DCX4 elements.

### 2.5 FEA validation

2.5.1 Macrographs

A macrograph of each weld with the weld beads intact was captured using a Canon EOS 550D DSLR camera. The macrographs, an example of which is shown in Fig. 3, were

Fig. 1 Sketch of welded HDPE pipe section showing the location of the weld, with the melt zone and the weld beads in *red* (**a**) and the specimen for NI enclosed in the *box* (**b**), where the location of the indentation grid is highlighted by the *orange rectangle* 6 × 0.3 mm, placed at the centre of the pipe wall

Fig. 2 Positioning methodology of the nanoindentation grid
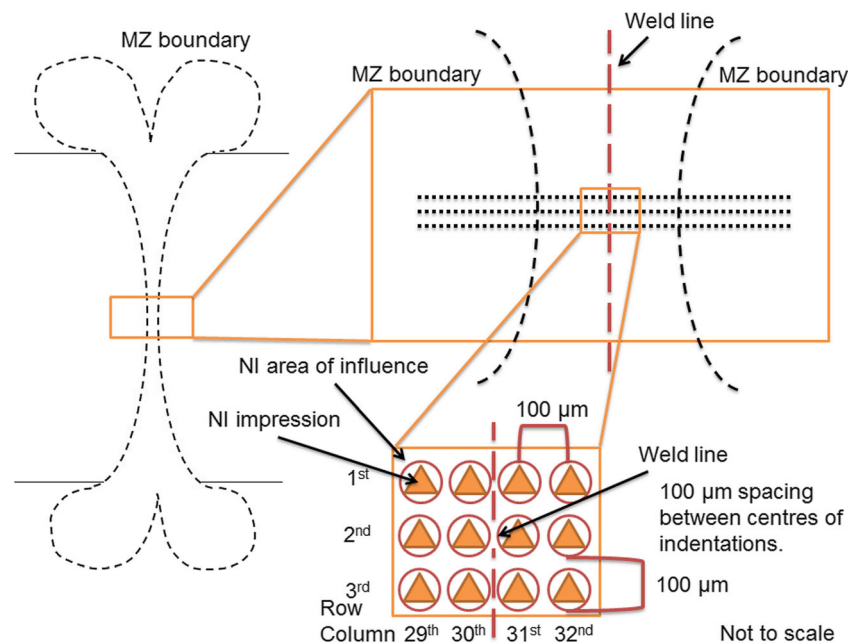
used to calculate the area of the weld beads that form from the material ejected from the pipe walls. The melt zone, whilst optically visible, was difficult to capture in the macrograph without being marked by a knife edge.

2.5.2 Microtomy

Microtomy is a useful technique to obtain thin slices of fairly consistent thickness. The specimens were cut using a Leica RM 2155 microtome. A disposable tungsten carbide knife was used to produce 20 ± 5-μm-thick slices across the weld with an area of 7 mm wide by 5 mm tall for transmission light microscopy (TLM). For the differential scanning calorimetry (DSC), microtomy was used to produce two 50 ± 5-μm-thick slices with an area of 10 mm tall by 10 mm deep for the weld and the parent regions. The locations of microtomed slices are shown in Fig. 3.

2.5.3 TLM

An Olympus BH-2 transmission light microscope with a QImaging Retiga 2000R camera was used to image the microtomed slices. The polarised light was rotated until the

Table 3 Nanoindentation experiment parameters

Parameter	Value	Unit
Indenter	Berkovich	–
Load	150	mN
Speed	10	μm/min
Hold time	15	s
Displacement (estimated)	12.5	μm

contrast due to the difference of orientation of the crystalline regions between the parent material and the weld was visible. Owing to the asperity in the slice thickness, the images required digital post-processing to improve their contrast and colour balance.

2.5.4 DSC

DSC is used for studying the thermal behaviour of materials during a phase change. A TA Instruments Q2000 DSC
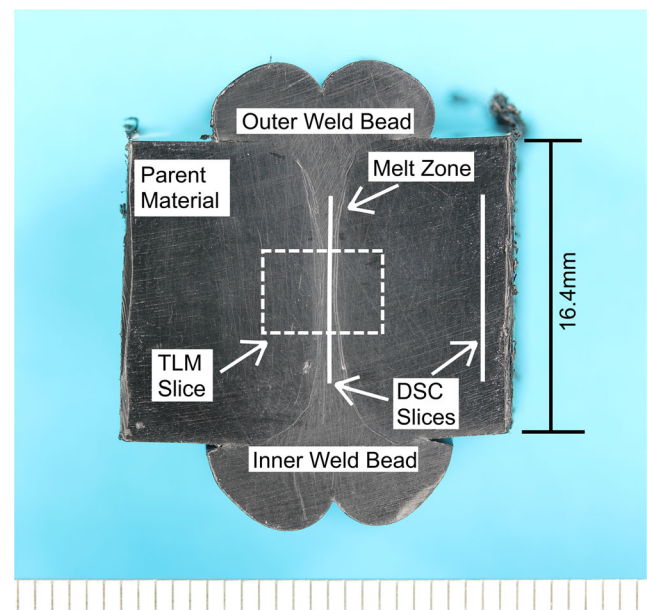

Fig. 3 Typical macrograph of a weld sample with the visible weld features labelled and locations of slices to be microtomed mapped

Table 4 Nanoindentation-derived parent material properties for each welding procedure

Welding procedure	Hardness (GPa)	Elastic modulus (GPa)
WP1	0.052	1.34
WP2	0.057	1.42
WP3	0.052	1.34
WP4	0.053	1.34
WP5	0.056	1.36
WP6	0.054	1.36
Average	0.054	1.36

was calibrated using indium following the manufacturer's recommended procedure for a temperature range of 20–180 °C. For the calculation of crystallinity, the specific heat of fusion was taken to be 293.6 J/g for 100% crystalline HDPE [11, 12]. Each DSC run was conducted with a heating rate of 10 °C/min and a cooling rate of 5 °C/min. The heat of fusion for each run was calculated by integrating between 80 and 140 °C [13].

3 Results and discussion

3.1 Nanoindentation

The parent material properties averaged across all welding procedures are 0.054 GPa with a standard deviation of 0.002 GPa for the hardness and 1.36 GPa with a standard deviation of 0.03 GPa for the elastic modulus. Table 4 lists

the parent material properties for each procedure, where it can be seen that the NI-derived elastic modulus is 24% higher than the tensile modulus reported by the pipe manufacturer, possibly due to the different strain rates used during the tests [10, 14]. However, in this work, nanoindentation was only used to study general trends rather than absolute values.

Figures 4, 5, 6, 7, 8 and 9 show the hardness (solid white) and elastic modulus (solid grey) values across the butt fusion weld for each of the six welding procedures overlaid with the TLM images at the same scale. The change in crystal orientation in the MZ is visible either as a discoloured region or contained within sharp edges, when using polarised light in TLM images. These graphs show very good correlation between the position of the peaks in both hardness and elastic modulus and the boundary of the MZ. Inside the MZ, there is a sharp reduction in hardness and elastic modulus, whereas outside the MZ, there is a more gradual decrease in properties until they level out to the parent material values. Therefore, nanoindentation suggests that the influence of heat dissipation from the melt zone extends much further into the parent material than the MZ, forming a second boundary, the heat-affected zone (HAZ). It should be noted that the HAZ boundary cannot be seen in the TLM image, as the heat flux is insufficient to alter the material optically. There is a distinct twin-peak pattern of increase in the material properties across the weld region, marking the MZ boundaries. The material properties at the peaks are 5–6% higher than for the parent material for each welding procedure. The individual values of hardness and elastic modulus at both peak positions are listed in Table 5.

The NI technique is very sensitive to surface perturbations [15–17]; therefore, the results reported were averaged from

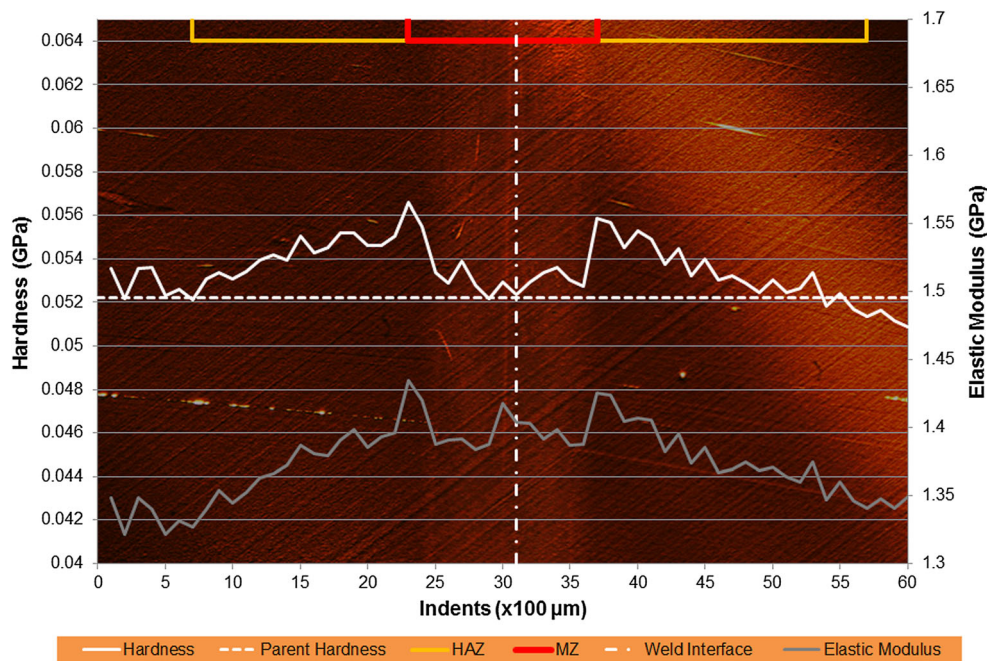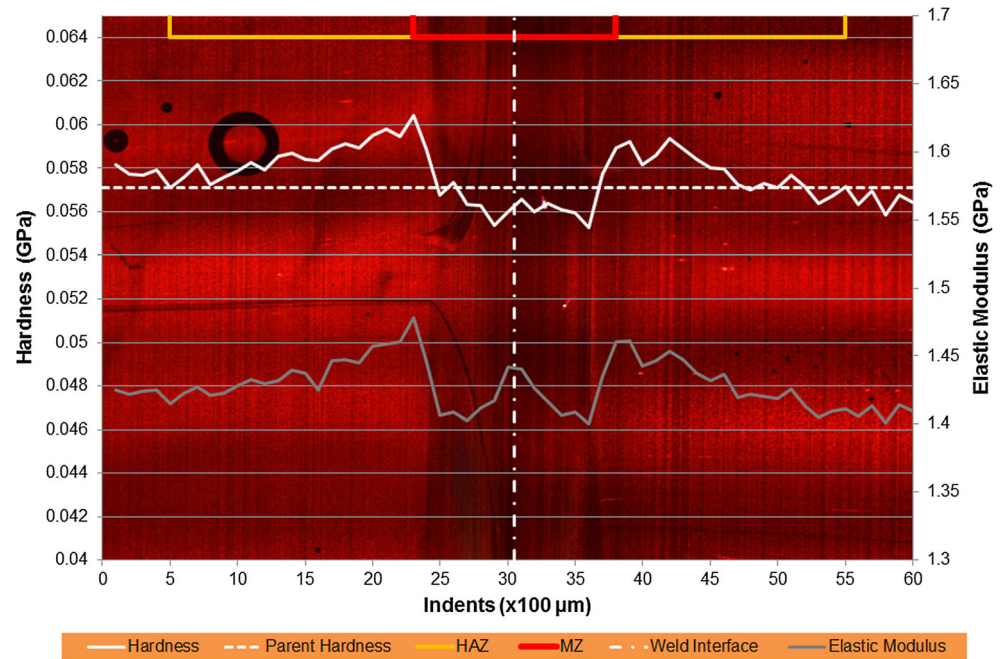**Fig. 4** Nanoindentation chart overlaid with TLM images for WP1

Fig. 5 Nanoindentation chart overlaid with TLM images for WP2

the three indentation rows. The scatter could have been re-duced further by using larger loads. However, this would be at the expense of spatial resolution since the indents would be larger, and therefore, the distance between them would need to be increased.

3.2 DSC

The material for DSC was extracted from the parent and weld region of WP1. It is expected that the crystallinity of the MZ at the weld interface would be similar for the different welding procedures as the welding process heats the material above the melting temperature. The DSC heating plots for the parent pipe and the weld (WP1) regions are shown in Fig. 10. The calculated crystallinity for the parent material was 63.8% and for the weld material was 67.8%. The onset of melting begins at 80 °C as the shorter polymer chains and other low molecular weight molecules loosen. The reduction in heat flow accelerates at approximately 100 °C for the parent and 105 °C for the weld.

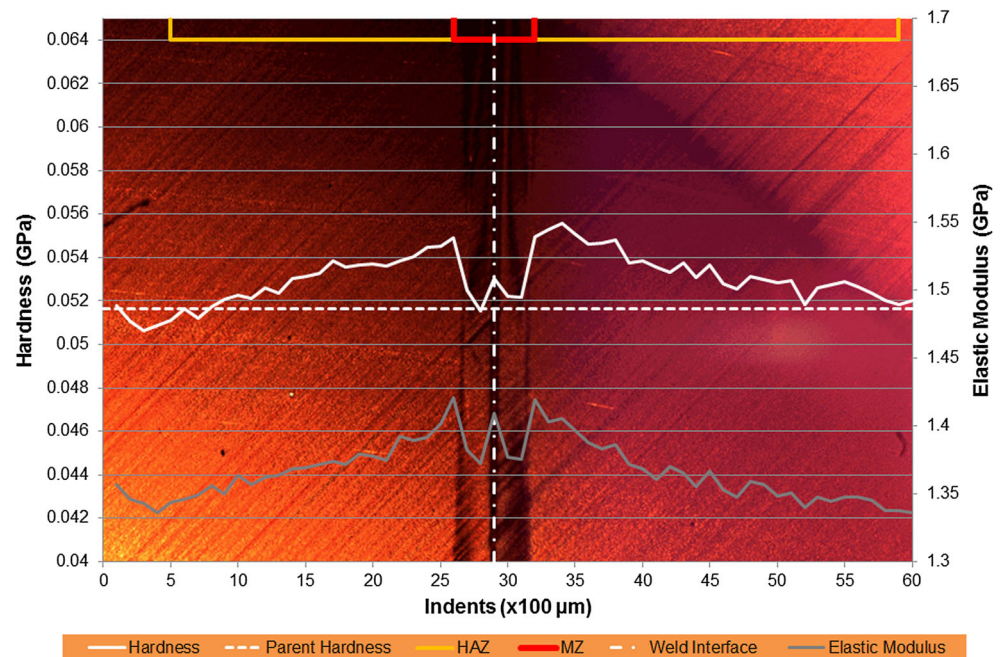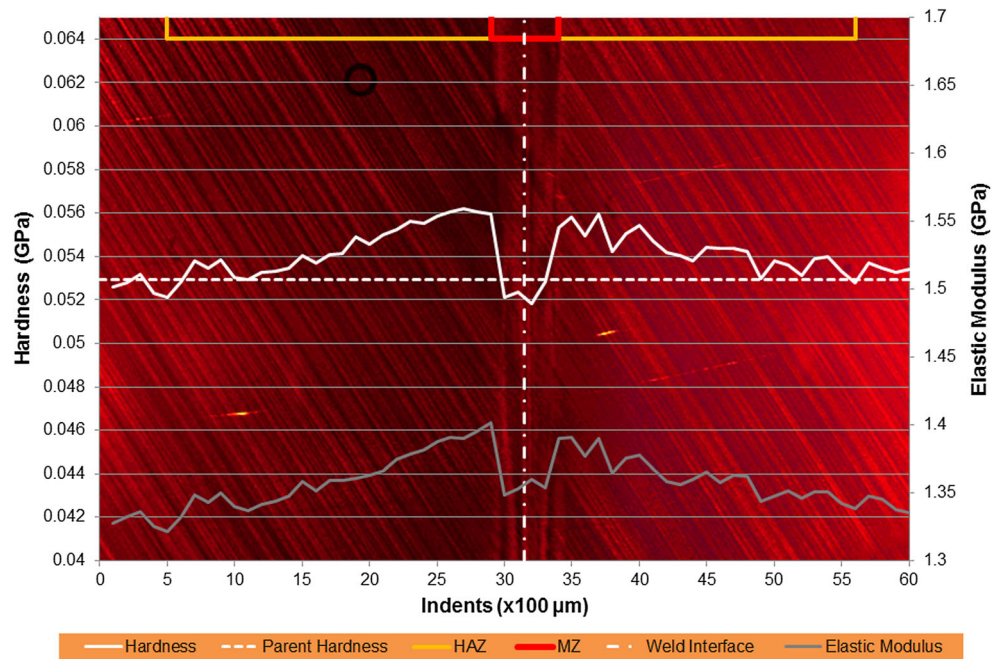**Fig. 6** Nanoindentation chart overlaid with TLM images for WP3

Fig. 7 Nanoindentation chart overlaid with TLM images for WP4

3.3 FEA

A typical thermal profile from the FEA analysis is shown in Fig. 11 with a representation of the heater plate superimposed for illustrative purposes. The effect of the different welding procedures can be observed by extracting the values of temperature versus distance from the heater plate from the FEA models at the end of the heating stage (Fig. 12), where the dotted horizontal line marks the melting point, as obtained from the DSC curves from the parent pipe. From Fig. 12, it

can be seen that WP1 has the shortest depth of molten material from the weld interface, followed by WP2. Despite having a wide range of heater plate temperatures, the remaining four procedures all have similar melt depths of around 8 mm.

A complete picture of the welding cycle for the different welding procedures is mapped in Fig. 13 with colour-coded temperature ranges, which allow for an easier comparison of how far the heat has travelled into the pipe and how long it took. The data for all procedures was extracted from a 25-mm-long path at the centre of the pipe wall, and the model was

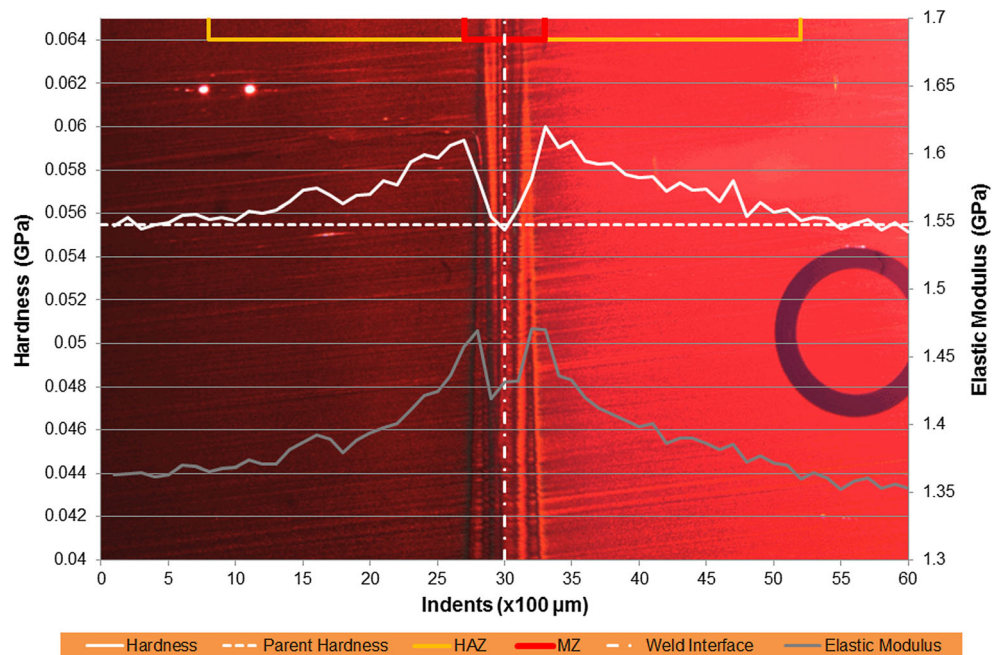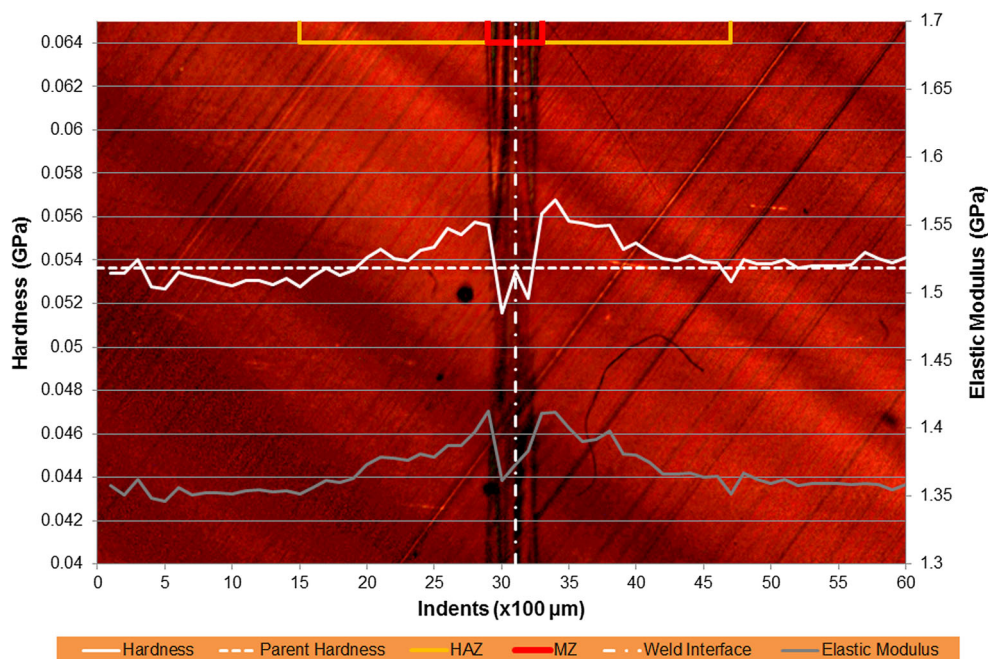**Fig. 8** Nanoindentation chart overlaid with TLM images for WP5

Fig. 9 Nanoindentation chart overlaid with TLM images for WP6

continued to run for extra 600 s to include the cooling stage. The red region indicates where the material temperature was over 128 °C. It can be seen from Fig. 13 that for WP3 and WP6, the depth of the material above 128 °C, i.e. the undeformed melt zone, increases slightly after the end of the heating stage as the heat transfers from the hot to the cold regions.

The maximum distances into the HDPE material that reached the melting point, for the six different welding procedures, were determined from Fig. 13 and were doubled in order to determine the width of the undeformed MZ. These values are given in Table 6 and were used to calculate the area of the undeformed MZ, which were then compared against the measured area of the deformed melt zone and welds beads, in order to verify the FEA models.

Table 5 Hardness and elastic modulus values for the two peak positions with a percentage increase against the parent material value in the brackets, for each welding procedure

Welding procedure	Hardness, GPa (%)		Elastic modulus, GPa (%)	
Position	Peak 1	Peak 2	Peak 1	Peak 2
WP1	0.057 (8.4)	0.056 (7.0)	1.44 (7.0)	1.43 (6.4)
WP2	0.060 (5.8)	0.059 (3.3)	1.48 (4.4)	1.46 (3.2)
WP3	0.055 (6.3)	0.055 (6.4)	1.42 (5.8)	1.42 (5.7)
WP4	0.056 (5.7)	0.055 (4.5)	1.40 (5.0)	1.39 (4.1)
WP5	0.059 (7.1)	0.060 (8.1)	1.46 (7.2)	1.47 (8.1)
WP6	0.056 (3.9)	0.057 (5.8)	1.40 (4.2)	1.41 (4.1)
Average	0.057 (6.2)	0.057 (5.8)	1.43 (5.6)	1.43 (5.2)

3.4 Melt zone

Although the FEA model did not account for deformation of the melt, it can be used to estimate the amount of material that is melted by the heater plate. Figure 14 shows a schematic of the MZ in the undeformed state, as calculated using the FEA model (Fig. 14a), and also in the actual deformed state observed in the welded samples (Fig. 14b). The area of the FEA MZ was calculated using the width of the undeformed MZ (W_F) from Table 6. The area of the MZ from the welded samples was calculated by measuring the area of the weld beads from the macrographs and the area of the visible MZ from the TLM images. The comparison of the two is shown in Table 7, which shows that there is a good correlation between the MZ areas as determined from the thermal FEA models and from the measurement of the actual welds themselves. This correlation whilst validating the FEA models also could be improved by modelling the effect of interfacial pressure. Such an effect would subject the parent material to a sharper temperature gradient as the molten material is pushed outwards into the weld beads. The material in the weld bead would also cool faster than the MZ material due to larger external surface area from which to transfer the heat into the ambient environment.

A comparison of the deformed melt zone widths (W_D) determined from TLM and NI is given in Table 8, which shows a reasonable correlation between the two different methods. This correlation could be improved by increasing the spatial resolution of the NI grid, which was limited to 100 μm in the current study. It is also recommended that TLM images are used to better position and optimise the layout of the nanoindentation grid across the MZ region.

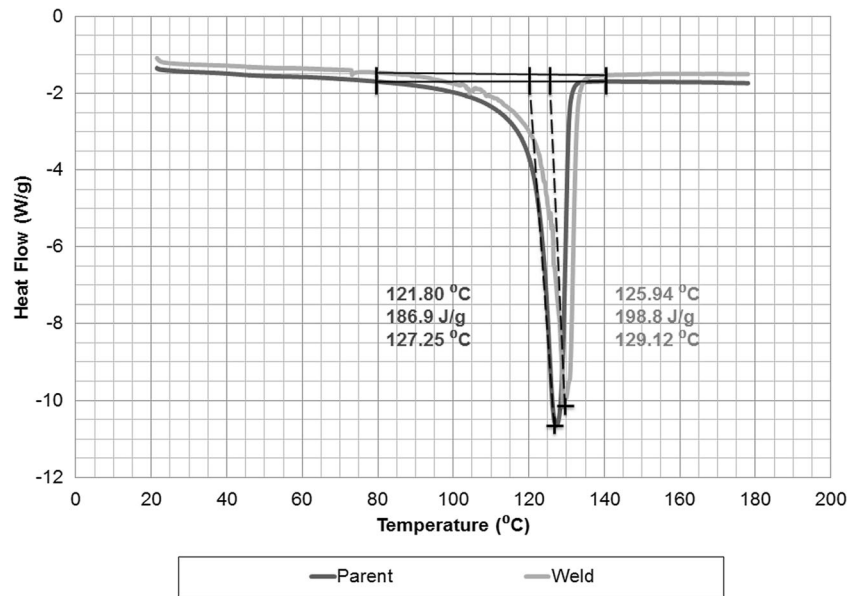**Fig. 10** Resulting plot of DSC for the parent and the weld (WP1) regions

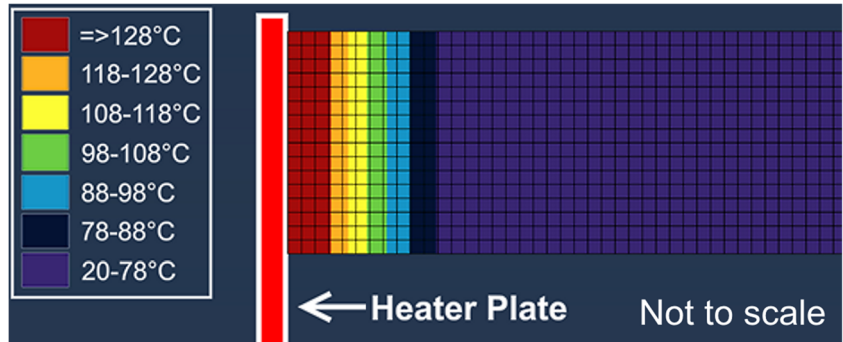**Fig. 11** Thermal profile from the FEA model

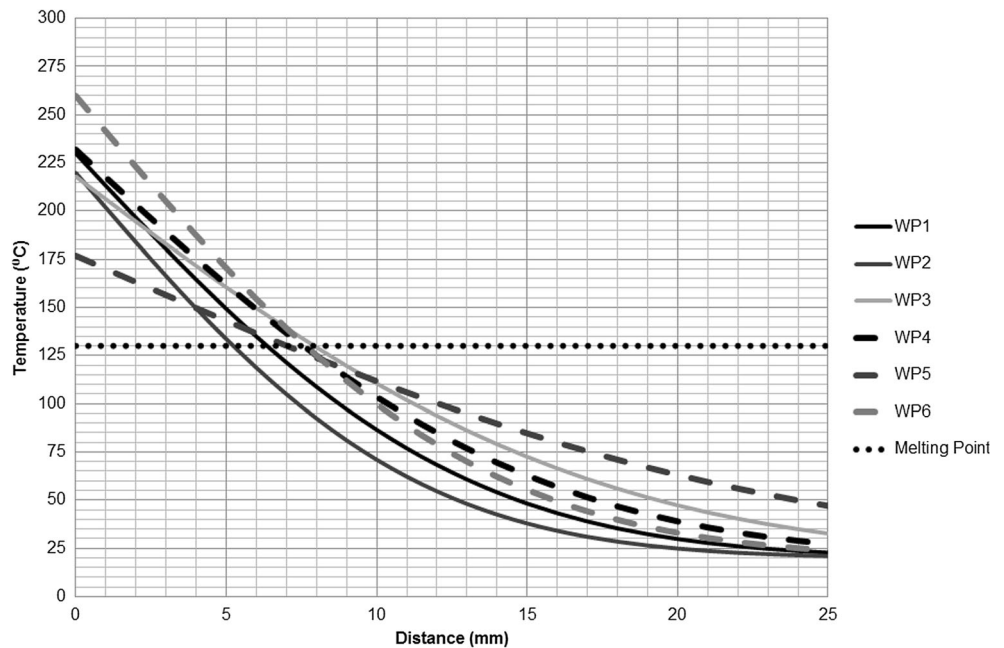**Fig. 12** Temperature profile for each welding procedure at the end of the heating stage
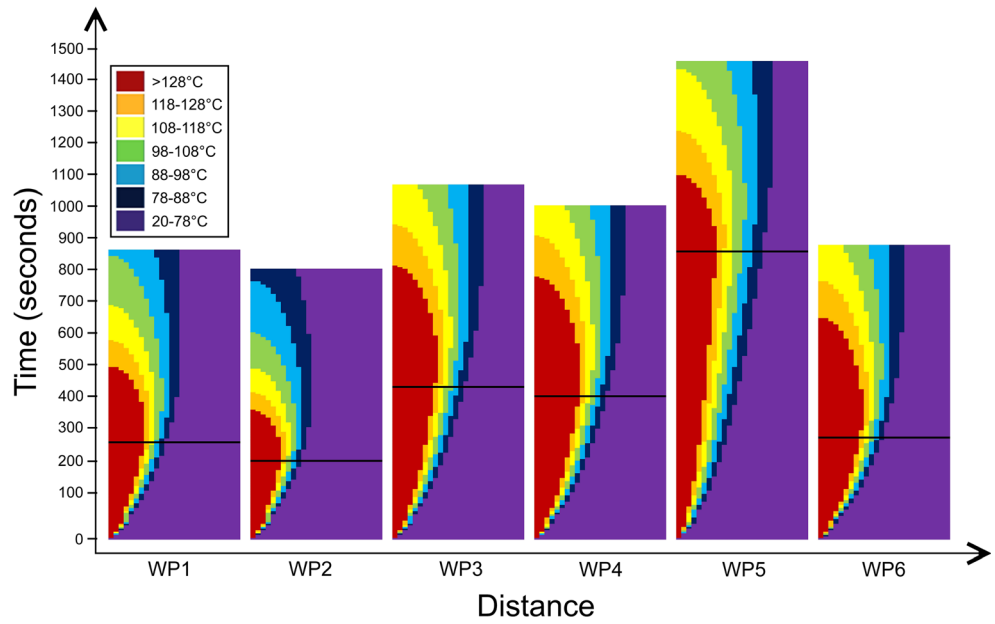
Fig. 13 Temperature profiles for each procedure plotted on distance against time axes WIS 4–32-08 (WP1), DVS 2207–1 (WP2), PPI TR-33 ideal (WP3), PPI TR-33 acceptable (WP4), high pressure low temperature (WP5) and high pressure high temperature (WP6). The end of the heating stage is marked by a *black line* for each procedure


3.5 Heat-affected zone

Despite not being observed optically, the existence of the HAZ was indicated by the nanoindentation results. The micro-mechanical properties peaked at the boundary of the MZ and then decreased gradually moving away from the MZ, until matching the parent material properties. This increase in micro-mechanical properties compared to the parent material shows that, although not melted, the material in this region (the HAZ) has been annealed.

The thermal data obtained from the FEA models have been used to highlight the areas in Fig. 13 above 80 °C, which is approximately the onset of melting from DSC, and below 128 °C, the melting point from the DSC (Fig. 10). Annealing of HDPE material causes increase in certain mechanical properties such as hardness and elastic modulus via promoting the growth of crystallite regions and in turn increasing the overall crystallinity of the region [18–20]. The strength of the effect of annealing is dependent on the magnitude of the temperature between

Table 6 Calculated undeformed width of MZ, W_F, from thermal FEA models for the different welding procedures

Welding procedure	FEA width at MZ (W_F), mm
WP1	12.1
WP2	10.0
WP3	15.8
WP4	15.9
WP5	14.7
WP6	14.3
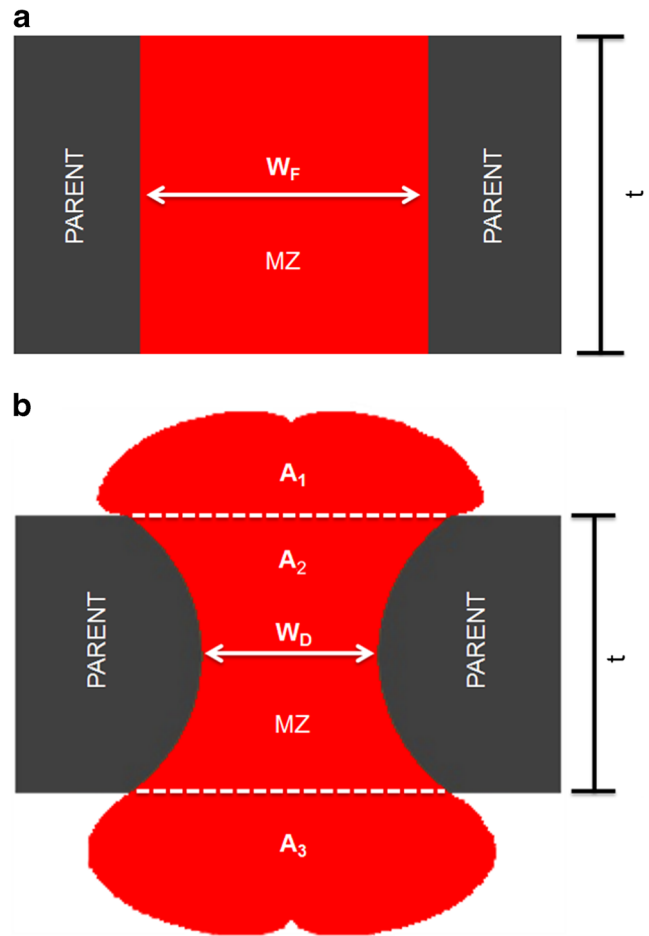
$$MZ\ Area\ from\ FEA = W_F \times t$$

$$Actual\ MZ\ Area = A_1 + A_2 + A_3$$

Fig. 14 Relative size of MZ in **a** undeformed state and **b** deformed state

Table 7 Calculation of MZ areas from FEA and measurements

| Welding procedure	Macrography + TLM-measured area (1) + (2) + (3), mm^2	FEA area (A), mm^2
WP1	173	198
WP2	160	164
WP3	280	259
WP4	284	260
WP5	233	240
WP6	216	234

Table 8 Comparison of the deformed MZ widths (W_D) as determined from results of the TLM and the NI for the different welding procedures

Welding procedure	Melt zone width (W_D), (mm)	
	From TLM	From NI
WP1	1.15	1.40
WP2	1.04	1.50
WP3	0.45	0.60
WP4	0.43	0.50
WP5	0.40	0.60
WP6	0.43	0.40

Table 9 HAZ widths listed by the techniques and the welding procedures

Welding procedure	Heat-affected zone width (mm)	
	From NI	From FEA[a]
WP1	3.6	3.0
WP2	3.5	2.0
WP3	4.8	4.8
WP4	4.6	4.4
WP5	3.8	7.5
WP6	2.8	3.5

[a] Assuming that the HAZ boundary reached a temperature of 105 °C during welding
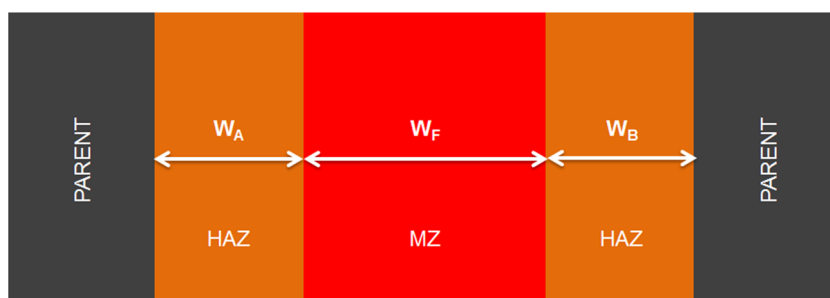
80 and 128 °C and the length of time the material was at that temperature. Table 9 shows a comparison of HAZ width as determined from the NI results and from the thermal FEA models, assuming that the HAZ boundary reached a temperature of 105 °C during welding, where the definition of HAZ width is given in Fig. 15. This temperature value was found to give the best correlation between the NI and thermal FEA results.

It can be seen from Table 9 that the FEA model grossly underestimated the HAZ width for WP2 and greatly overestimated the HAZ width for WP5. The differences between the thermal FEA models and NI results for the HAZ width are probably due to the heat loss not being accounted for in the modelling and coarse spatial resolution in the NI results. WP2 had the smallest value of HAZ width from the thermal FEA model. This is probably due to WP2 having a 60-s shorter heat soak time and 10 °C lower heater plate temperature than WP1; these differences produced the smallest amount of molten material for the MZ and therefore less overall heat flux, which would lead to a smaller HAZ width as well. The molten material in the MZ acts as a heat reservoir for the HAZ; higher interfacial pressures reduce the size of the MZ reservoir by ejecting the material into the weld beads. WP5 had the largest value of HAZ width in the FEA model, which may be due to the fact that it had the longest heat soak time.

The size of the MZ is smallest at the centre of the pipe wall and widens as it gets closer to the pipe surface as seen in Fig. 3. This effect is difficult to see in the TLM images as the 7 × 5-mm slices were microtomed from the centre of the 16.4-mm-thick pipe wall, whilst the effect is more pronounced nearer the pipe surfaces. It is also possible that the HAZ expands in a similar manner, but further work is required to verify this possibility. Work of several researchers has been reviewed by Rashid [21], where the weld geometry is limited to the various features or zones identified using optical means within the MZ. However, based on the NI results given here, a new weld geometry can be proposed for butt fusion joints in HDPE pipes which appropriately acknowledges the optically invisible components of the weld region, as illustrated in Fig. 16 assuming a consistent HAZ width from the pipe surface to the pipe bore.
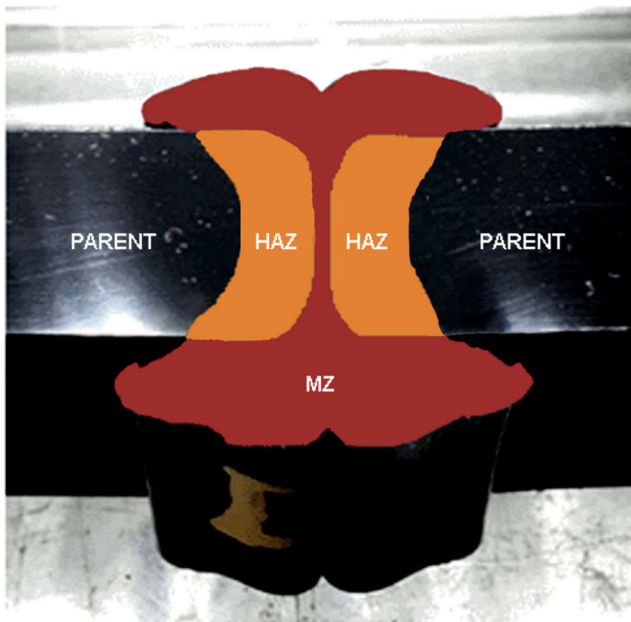
Fig. 15 Illustration of the HAZ width in an undeformed state

$$HAZ\ Width = W_A + W_B$$

Fig. 16 Proposed MZ and HAZ in a butt fusion-welded HDPE pipe

4 Conclusions

The nanoindentation technique has been proven to be a valuable tool in characterising the variation in the material properties across butt fusion welds in HDPE pipes. The results show that butt fusion welds have a melt zone, where the material was melted during the welding operation, and also have a heat-affected zone, where the material was annealed, resulting in an increase in micro-mechanical properties. A thermal FEA model has been used to suggest that the HAZ boundary is where the material temperature reached around 105 °C during the welding operation.

5 Recommendations

This work has only investigated the weld at the centre of the pipe wall. It would be useful to explore the change in the structure and material properties closer to the pipe wall surfaces.

The methodology of nanoindentation itself can be improved via reduction in surface roughness.

A more detailed FEA simulation, taking into the account the deformation of the MZ and HAZ, due to pressure would enhance the accuracy of the models used for predicting the size of both zones.

A technique such as DSC with microtomy to correlate crystallinity with NI across the weld region for the different welding procedures would provide a spatial resolution of 50 μm, double the spatial resolution of the NI grid.

It is also suggested that it would be useful to investigate the effects of post-weld heat treatment of the butt fusion-welded HDPE pipes based on the proposed weld geometry in order to improve weld strength and performance.

References

1. Ceresana, Market Study (2013) Plastic pipes—Europe, 2nd edn. Ceresana, Konstanz
2. Ezekoye OA, Lowman CD (1998) Polymer weld strength predictions using a thermal and polymer chain diffusion analysis. Polymer Eng Sci 38(6)
3. Fischer-Cripps T, Anthony C (2010) Nanoindentation, 2nd edn. Springer, New York
4. Qian L, Li M, Zhou Z, Yang H, Shi X (2005) Comparison of nanoindentation hardness to microhardness. Surf Coat Technol 195:264–271
5. Sattler K, Feng Z-Q, He Q-C, Zeng Q, Joli P (2010) Theory of nanoindentation. In: Handbook of Nanophysics. Taylor and Francis
6. Poon B, Rittel D, Ravichandran G (2008) An analysis of nanoindentation in linearly elastic solids. Int J Solids Struct 45:6018–6033
7. Borealis Group (2013) HE3490LS product datasheet
8. TWI (2014) FAQ: standards used for PE pipes. [Online]. Available: http://www.twi-global.com/technical-knowledge/faqs/standards-faqs/faq-standards-used-for-polyethylene-pipe/. Accessed 06 2014
9. Cheng Y-T, Cheng C-M (2004) Scaling, dimensional analysis and indentation measurements. Mater Sci Eng 44:91–149
10. Oyen ML, Cook RF (2002) Load-displacement behaviour during sharp indentation of viscous-elastic-plastic materials. J Mater Res 18(1):139–151
11. Leskovics K, Kollar M, Barczy P (2006) A study of structure and mechanical properties of welded joints in polyethylene pipes. Mater Sci Eng A 419:134–143
12. Joshi M, Butola BS, Simon G, Kukaleva N (2006) Rhelogical and viscoelastic behavior of HDPE/octamethyl-POSS nanocomposites. Macromolecules 39(5):1839–1849
13. Jordens K, Wilkes GL, Janzen J, Rohlfing DC, Welch MB (2000) The influence of molecular weight and thermal history on the thermal, rheological, and mechanical properties of metallocene-catalyzed linear polyethylenes. Polymer 41:7175–7192
14. Huang Y, Zhang F, Hwang KC, Nix WD, Pharr GM, Feng G (2006) A model of size effects in nano-indentation. J Mech Phys Solids 54: 1668–1686
15. Zhang YW, Zhang CY, Zeng KY, Shen L (2005) Nanoindentation of polymers with a sharp indenter. J Mater Res 20(6):1597–1606
16. Rocha JR, Yang KZ, Hilbig T, Brostow W, Simoes R (2013) Polymer indentation with mesoscopic molecular dynamics. Mater Res Soc 28(21):3043–3052
17. Rodriguez SA, Alcala J, Souza RM (2012) The reduced modulus in the analysis of sharp instrumented indentation tests. J Mater Res 27(16):2148–2161

18. Krishnaswamy RK (2005) Analysis of ductile and brittle failures from creep rupture testing of high-density polyethylene (HDPE) pipes. Polymer 46(25):11664–11672

19. Janzen J, Register DF (1996) Crystallinity dependence of modulus and yield properties of polyethylenes. J Eng Appl Sci 2:2190–2194

20. Göritz D, Kemmerer J, Kreitmeier S, Rossbacher R (1983) Annealing effects in high modulus polyethylene. Colloid Polym Sci 261:631–634

21. Rashid H (1997) Butt fusion welding of polyethylene pipes. Brunel University